occurs at a point where the density of two-phonon states vanishes. The existence of this anomalous structure may be a resonance effect which emphasizes scattering by two phonons near Γ. The $\Gamma_{25'}$ spectrum can be understood in terms of two-phonon overtone and combination states, while the Γ_{12} spectrum is seen to be relatively unimportant.

ACKNOWLEDGMENTS

We would like to thank Dr. R. Reed for suggesting the He purging of the sample, Professor H. Bilz for discussions concerning the $\Gamma_{15'}$ Raman components, and Professor C. E. Hathaway for a preprint of his work.

*On leave from Brown University, Providence, R. I. 02912.

[1]J. H. Parker, Jr., D. W. Feklman, and M. Askin, Phys. Rev. 155, 712 (1967).

[2]B. A. Weinstein and Manuel Cardona, Solid State Commun. 10, 961 (1972).

[3]Paul A. Temple and C. E. Hathaway, Phys. Rev. B (to be published).

[4]Fernando Cerdeira and Manuel Cardona, Phys. Rev. B 5, 1440 (1972).

[5]F. Cerdeira, W. Dreybrodt, and Manuel Cardona, Solid State Commun. 10, 591 (1972).

[6]R. K. Ray, R. L. Aggarwal, and B. Lax, in *Light Scattering in Solids*, edited by M. Balkanski (Flammarion, Paris, 1971), p. 288.

[7]G. Nilsson and G. Nelin, Phys. Rev. B 3, 364 (1971).

[8]G. Nelin and G. Nilsson, Phys. Rev. B 5, 3151 (1972).

[9]Syton HT-50 colloidal solution, Monsanto Chemical Co., St. Louis, Mo. We are thankful to Dr. D. E. Aspnes for suggesting to us the use of this polishing etchant.

[10]R. A. Loudon, Adv. Phys. 13, 423 (1964).

[11]We have found no evidence for the antisymmetric tensor component $\Gamma_{15'}$. This component may become important for laser lines closer to the resonant E_1 or $E_1+\Delta_1$ gaps.

[12]R. Martin and T. C. Damen, Phys. Rev. Lett. 26, 86 (1971).

[13]P. Corden, A. Pinczuk, and E. Burstein, in *Proceedings of the Tenth International Conference on the Physics of Semiconductors, Cambridge*, 1970, edited by S. P. Keller, J. C. Hensel, and F. Stern (U. S. AEC, Oak Ridge, Tenn., 1970), p. 739.

[14]J. Renucci and F. Cerdeira (private communication).

[15]F. Cerdeira, W. Dreybrodt, and Manuel Cardona, in *Proceedings of the Eleventh International Conference on the Physics of Semiconductors, Warsaw* (Polish Scientific Publishers, Warsaw, 1972), p. 1142.

[16]B. Weinstein and M. Cardona (unpublished).

[17]J. F. Scott, T. C. Damen, R. C. C. Leite, and W. T. Silfvast, Solid State Commun. 7, 953 (1969).

[18]S. A. Solin and A. K. Ramdas, Phys. Rev. B 1, 1687 (1970).

[19]J. F. Angress and A. J. Maiden, J. Phys. C 4, 235 (1971).

[20]J. E. Smith Jr., M. H. Brodsky, B. L. Crowder, M. I. Nathan, and A. Pinczuk, Phys. Rev. Lett. 26, 642 (1971).

[21]R. A. Cowley, J. Phys. (Paris) 26, 659 (1965).

[22]A. D. Bruce and R. A. Cowley, J. Phys. C. 5, 595 (1972).

PHYSICAL REVIEW B VOLUME 7, NUMBER 6 15 MARCH 1973

Impact Ionization, Breakdown, and Photoinduced Switching in CdSe

R. P. Khosla, J. R. Fischer, and B. C. Burkey

Research Laboratories, Eastman Kodak Company, Rochester, New York 14650

(Received 11 September 1972)

Measurements of conductivity, Hall coefficient, and mobility of CdSe single crystals have been made in the temperature range 4.2–300 °K. For the sample with the lowest carrier concentration of 2.8×10^{15} cm^{-3}, the donor ionization energy of 18 meV is obtained. This is in good agreement with the calculated hydrogenic value of 19 meV. Above 100 °K, the electron–polar-optical-phonon interaction determines the mobility. Below 100 °K, ionized- and neutral-impurity scattering also contribute to the mobility, and for $T < 50$ °K dominate the mobility. At relatively low fields, nonlinear I-V characteristics are observed. The samples show breakdown around 100 V/cm (varies somewhat with carrier concentration), resulting in a region of current-controlled negative resistance. The conductivity, Hall coefficient, and mobility of the samples are measured in the high-field region. The samples which show current-controlled negative resistance can be switched from a low- to a high-conductivity state under illumination below the threshold field in the dark. The higher the intensity of illumination, the lower is the threshold field for switching. These results are discussed in terms of various models.

I. INTRODUCTION

Impact ionization of shallow donor and acceptor states has been observed in several semiconductors, namely, Ge,[1–3] GaAs,[4,5] and CdS.[6] Experimentally, a rapid increase in current is observed at a threshold electric field. In those cases for which the Hall coefficient can also be measured,

a rapid decrease in the Hall coefficient is observed along with the rapid current increase. This indicates an enhancement of the free-carrier density. This type of breakdown is found in extrinsic semiconductors only and occurs at a sufficiently low temperature so that most of the carriers are frozen into either localized states or a very low-mobility impurity band. A moderate electric field, then, will impart sufficient energy to those few remaining free carriers to result in impact ionization of the localized impurity states, resulting in an enhanced current, since the free carriers have a much higher mobility.

Under certain conditions, the breakdown resulting from impact ionization of shallow donor or acceptor states is accompanied by a region of current-controlled negative resistance (CCNR). This has been observed in GaAs[3,4] and Ge.[2]

Crandall[7] found that the photosensitivity of GaAs is enhanced if the sample is biased into the CCNR region. Qualitatively, the effect is not photoelectric gain in the usual sense, but instead, a photoinduced switching into the high-current state, which is possible only because of the occurrence of CCNR.

The present paper is a report of the low-field-transport, breakdown, CCNR, and photoinduced-switching measurements on several n-CdSe single crystals. Section II is a description of the experimental details. Section III contains the experimental results and analysis of the low-electric-field data. Section IV contains the experimental results and discussion of the dark high-electric-field data. Section V contains the results of photoinduced switching. Finally, Sec. VI is a discussion of some of the aspects of impact ionization of shallow donor states in semiconductors, and the CCNR that may occur in some of the cases.

II. EXPERIMENTAL DETAILS

Ultrahigh-purity single crystals of CdSe were obtained from the Eagle-Picher Co. Samples were cut either in the form of bars or spider shapes. Most of the samples were oriented with their c axis perpendicular to their plane. Some samples were cut with their c axis parallel to their plane. The lengths of the samples varied from 1.0 to 10 mm, they were 1–2 mm wide and their thicknesses varied from 0.35 to 1.0 mm. The samples were lapped and then etched in a solution formed by dissolving potassium permanganate in concentrated sulphuric acid.[8] This etch leaves no surface deposits. Indium contacts were soldered ultrasonically, which provide satisfactory low-resistance Ohmic contacts.

Standard four-probe dc potentiometric measurements were done on spider-shaped samples to determine their resistivities, Hall coefficients, and mobilities. High-field measurements were made using pulsed voltages from a Rutherford pulse generator, the range of which was limited to 80 V. Higher voltages were provided by a Velonex pulse generator model No. 350. A dual-beam oscilloscope with a 1A7 differential preamplifier was used in our studies. A Varian 6-in. electromagnet provided the necessary magnetic field for the Hall measurements.

For photoconductivity experiments, the light sources were (i) for dc measurement, a Bausch and Lomb monochromator using a tungsten source; (ii) for transient measurements, a xenon flashlamp. The intensity of the xenon flashlamp could be varied by changing the discharge-capacitator energy.

III. LOW-FIELD RESULTS

Table I gives the values of the free-carrier concentration, resistivity, Hall coefficient, and Hall mobility of the samples. Measurements of these quantities were carried out over the temperature range 4.2–295 °K. Representative data for sample EPS-2 are shown in Fig. 1. The resistivity plot shows two activation energies: one for $T > 20$ °K, corresponding to the donor-ionization energy; and one for $T < 20$ °K, corresponding to thermally activated hopping conduction in the impurity band. The maximum in the Hall coefficient, which is indicative of impurity conduction, was observed in all samples. The carrier concentrations $n = 1/R_H e$, where R_H is the measured Hall coefficient for three of the samples ranging from the smallest to the largest room-temperature carrier concentration are shown in Fig. 2. The donor and acceptor concentration N_D and N_A, respectively, and the donor ionization energy $\mathcal{E}_D$ can be obtained from an analysis of both n and the mobility. Since the impurity conduction begins at a sufficiently high temperature, N_A cannot be reliably extracted from an analysis of n alone. The values of N_A for two of the three samples of Fig. 2 were chosen to fit the mobility. The values of N_D and $\mathcal{E}_D$ and β were then

TABLE I. Resistivity, Hall coefficient, and mobility of CdSe samples at room temperature.

Sample No.	$n \times 10^{16}$ (cm^{-3})	ρ (Ω cm)	R_H ($cm^3\ C^{-1}$)	μ ($cm^2\ V^{-1}\ sec^{-1}$)
171-S	0.28	4.49	2220	495
EPS-4	1.87	0.56	335	605
EPS-2	3.0	0.36	207	585
EPS-3	3.0	0.36	208	586
SWC-1	6.5	0.17	98	596
EPS-5C	7.2	0.15	88	605
EPS-7B	8.11	0.13	77	581
EPS-5	11.3	0.10	56	555

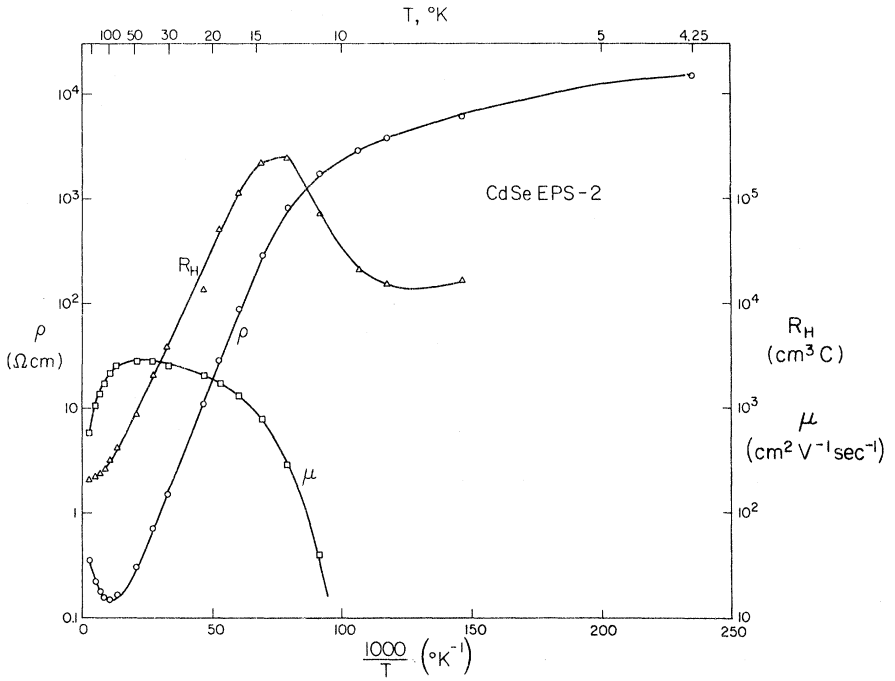

FIG. 1. Resistivity, Hall coefficient, and mobility vs $1/T$ for sample EPS-2.

obtained by fitting to the usual formula

$$\frac{n(n+N_A)}{N_D - N_A - N} = \beta N_c e^{-\mathcal{E}_D/kT} ,$$

where β is the degeneracy factor and N_c is the conduction-band density of states. Table II lists the values of the parameters found by this fitting procedure. The compensation is $K = N_A/N_D$. The sample with the lowest impurity concentration 171-S is the only case with $\beta = \frac{1}{2}$, which is the degeneracy factor expected for an isolated donor. The higher-concentration sample EPS-2 required a larger value of β and could not be fit well with $\beta = \frac{1}{2}$ for any values of N_A, N_D, and $\mathcal{E}_D$. This may be a result of the increasing overlap of the wave functions of adjacent donors. The largest concentration sample EPS-7B displayed some indication of impurity conduction at temperatures as high as

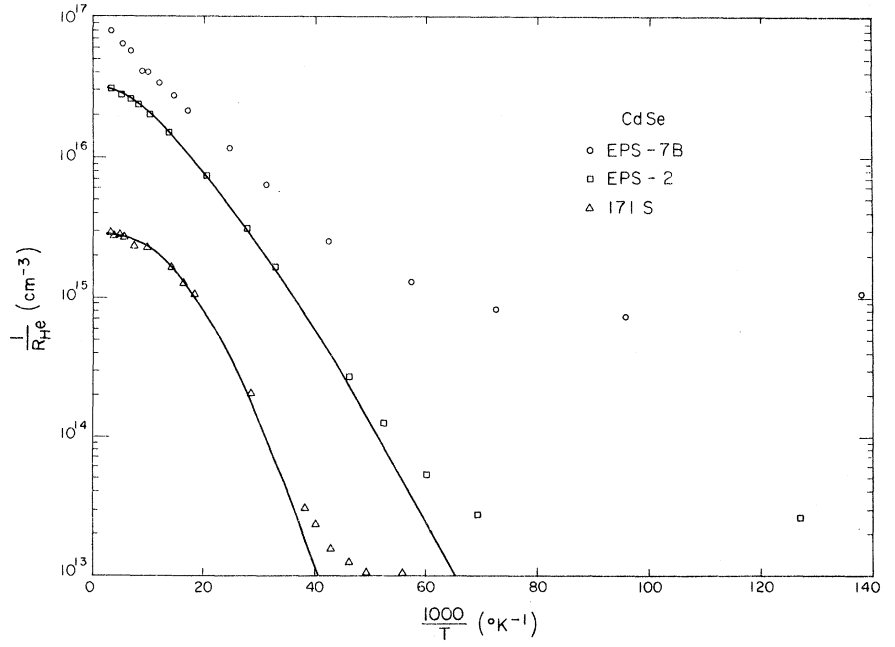

FIG. 2. $\ln(R_H e)^{-1}$ vs $1/T$ for three of the samples indicated. Solid lines through the data points are the theoretical fits as described in the text.

TABLE II. Values of N_A, N_D, $\mathcal{E}_D$, and β obtained from fitting the Hall coefficient and mobility data.

	171-S	EPS-2	EPS-7B
N_D	3.55×10^{15}	3.3×10^{16}	
N_A	7.5×10^{14}	1.4×10^{15}	
$\mathcal{E}_D$	18 meV	14.1 meV	10 meV (from R_H above 100 °K)
β	0.5	0.94	
K	21%	4.4%	

100 °K, and therefore could not be analyzed for N_D, N_A, and β.

The donor ionization energy may, however, be obtained from the high-temperature portion of the $\ln(eR_H)$-vs-T^{-1} plot, and is 10 meV for EPS-7B. Sample 171-S, with the lowest impurity concentration, had the highest ionization energy 18 meV. The effect of increasing the impurity concentration is to decrease the ionization energy. This effect is well known in Ge.[9] The observed donor-binding energies are consistent with those recently reported by others. Henry *et al.*[10] found $\mathcal{E}_D = 19.5 \pm 0.3$ meV from the analysis of the bound-exciton luminescence in CdSe and Burmeister and Stevenson[11] found $\mathcal{E}_D = 14$ meV for a CdSe sample with $N_A = 2\times10^{15}$ cm^{-3} and $N_D = 3.1\times10^{16}$ cm^{-3}, which is very similar to sample EPS-2. The hydrogenic value from $\mathcal{E}_D = (13.6)(m^*/m_e)/\epsilon_0^2$ is 19 meV. It should be emphasized that in every case reported, the donor in CdSe has not been identified.

The experimental Hall mobilities for the samples of Fig. 2 and the calculated drift mobilities for samples 171-S and EPS-2 are shown in Fig. 3. The mobilities are calculated on the basis of the electron-temperature model (ETM), for which the Hall and drift mobilities are the same. The electron scattering mechanisms included are (i) ionized impurities, (ii) neutral impurities, (iii) polar-optical phonons, (iv) acoustic phonons via the deformation potential, and (v) acoustic phonons via the piezoelectric potential. A discussion of the ETM and a list of the CdSe parameters are included in Appendix A. Above 100 °K, the electron interaction with the optical phonons determines the mobility. Below 100 °K, ionized- and neutral-impurity scattering also contribute to the mobility, and, for $T < 50$ °K, they dominate the mobility. A decomposition of the mobility for EPS-2 is shown in Fig. 4.

IV. DARK HIGH-FIELD RESULTS

High-field measurements on all the samples show that the samples obey Ohm's law at low fields, beyond which the current increases superlinearly with increasing field, and breakdown occurs around 100 V/cm (varies somewhat with carrier concentration), resulting in a region of negative resis-

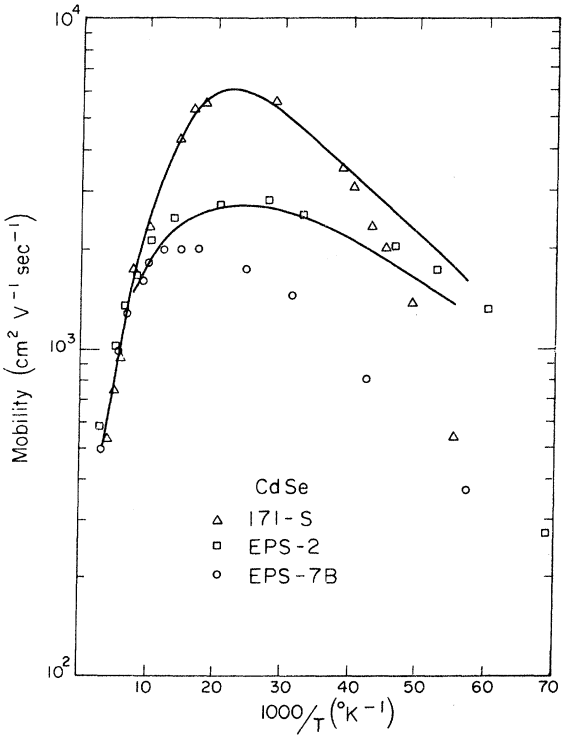

FIG. 3. $\ln\mu$ vs $1/T$ for the samples of Fig. 2. Solid lines through the data points are the mobilities calculated on the electron-temperature model (see text).

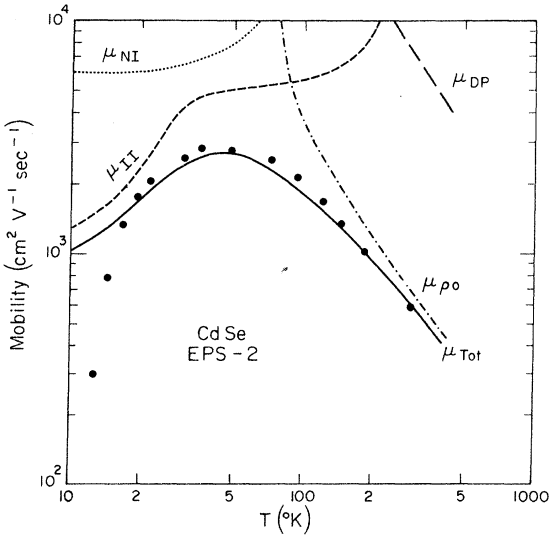

FIG. 4. Decomposition of the calculated mobility for sample EPS-2. μ_{II} represents the mobility due to ionized-impurity scattering, μ_{NI} is that due to neutral-impurity scattering, μ_{DP} is due to deformation potential, and μ_{PO} is that due to polar-optical scattering.

tance. Representative data for one of the samples are shown in Fig. 5.

Beyond the CCNR region, the current is the same at all temperatures. This behavior is similar to that reported for other materials.[3-5,12] No hysteresis effect is observed and the phenomenon of CCNR repeats itself, irrespective of the number of times the sample is subjected to pulsed voltage cycles.

The drop in voltage and the corresponding increase in current is concentration and temperature dependent. The maximum voltage drop occurs for a sample with carrier concentration of $\simeq 7\times 10^{16}$ cm^{-3}.

Figure 6 shows a plot of I vs E for various temperatures for sample EPS-7B. With increasing temperature, both the threshold field and the negative resistance decrease. Figure 7 shows the values of the two turning points plotted vs temperature. The breakdown field refers to the first turning point and the sustaining field to the second turning point. The difference between the two turning points decreases, and eventually the current rises without any CCNR. This observation is consistent with that reported by Zylbersztejn for p-Ge.

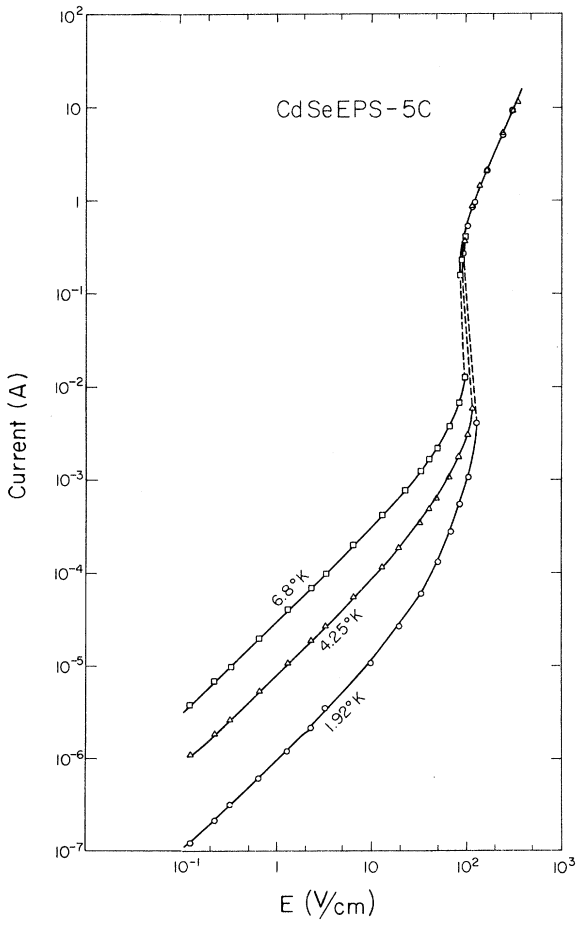

FIG. 5. Current vs applied field for another sample CdSe EPS-5C (C-axis parallel to the plane of the sample). Note that the negative resistance region is shown by dotted lines.

In the CCNR region, relaxation oscillations are observed. We were able to vary the frequency from 5 to 50 kHz depending on the value of capacitance and resistance in the circuit.

The conductivity, Hall coefficient, and the Hall mobility were measured vs the electric field. Representative data for one of the samples are plotted in Fig. 8.

No heating effects were noticeable with pulsewidths up to 200 μsec. The CCNR sets in at approximately the same field for a particular temperature, irrespective of the length or the area of the sample. The critical field for breakdown was also the same, whether it was determined from the voltage measured at the two ends or from the side arms of the spider-shaped samples. We therefore believe that the observed CCNR is a bulk effect and not an electrode effect. The effect is reproducible in different samples with the same carrier concentration.

Figure 2 showed that the samples possess characteristic impurity conduction. By a simple calculation using the two-band conduction formulas, it can be demonstrated that the Hall coefficient and conductivity data vs electric field plotted in Fig. 8 indicate that electrons are transferred from the low-mobility impurity states to the much higher mobility conduction band.

For two-band conduction, the conductivity σ and the Hall coefficient R_H are given by

$$\sigma = en_c\mu_c + en_i\mu_i \tag{1}$$

and

$$R_H^{-1} = \frac{e(n_c\mu_c + n_i\mu_i)^2}{n_c\mu_c^{H2} + n_i\mu_i^{H2}} \tag{2}$$

where n_c, μ_c, μ_c^H and n_i, μ_i, μ_i^H are the carrier concentration, mobility, and Hall mobility for the conduction band and the impurity band, respectively. It is plausible that μ_c will become field dependent at a lower field than does n_c or n_i. Suppose for the purpose of this qualitative argument that $\mu_c^H \approx \mu_c$ and $\mu_i^H \approx \mu_i$. If $\mu_c = \mu_c(E)$, and it is assumed that $n_i\mu_i^2 < n_c\mu_c^2$, then σ and R_H^{-1} can be differentiated with respect to E and are given by

$$\frac{d\sigma}{dE} = en_c\frac{d\mu_c}{dE} \tag{3}$$

and

$$\frac{d(R_H^{-1})}{dE} = -2e\frac{n_c}{\mu_c}\left(\frac{n_i\mu_i}{n_c\mu_c}+1\right)\frac{n_i\mu_i}{n_c\mu_c}\frac{d\mu_c}{dE}\ . \tag{4}$$

Note that the derivatives or the slopes of R_H^{-1} and

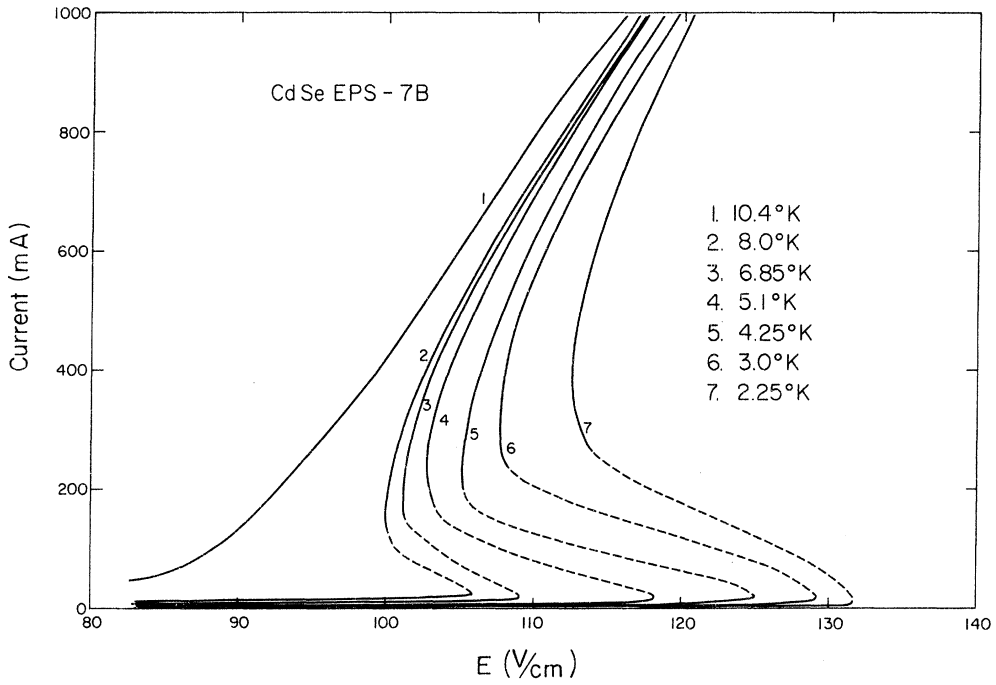

FIG. 6. Temperature dependence of the current vs applied field for one of the samples EPS-7B.

σ-vs-E curves are proportional to that of μ_c, but are of opposite sign. Thus, when σ starts to increase with E, R_H^{-1} starts to decrease. With increasing field, the carrier concentration in the conduction band increases as a result of impact ionization or other field-induced electron transfer from the impurity states to the conduction band. The conductivity will become dominated by the conduction band as n_c increases, and eventually the field dependence of n_c will control R_H^{-1}, the slope will become positive, and R_H^{-1} will rise rapidly. This is evidenced by our data in Fig. 8. At 4.2°K, σ starts to increase and R_H^{-1} decreases at approximately 25 V/cm. With further increase in E, σ

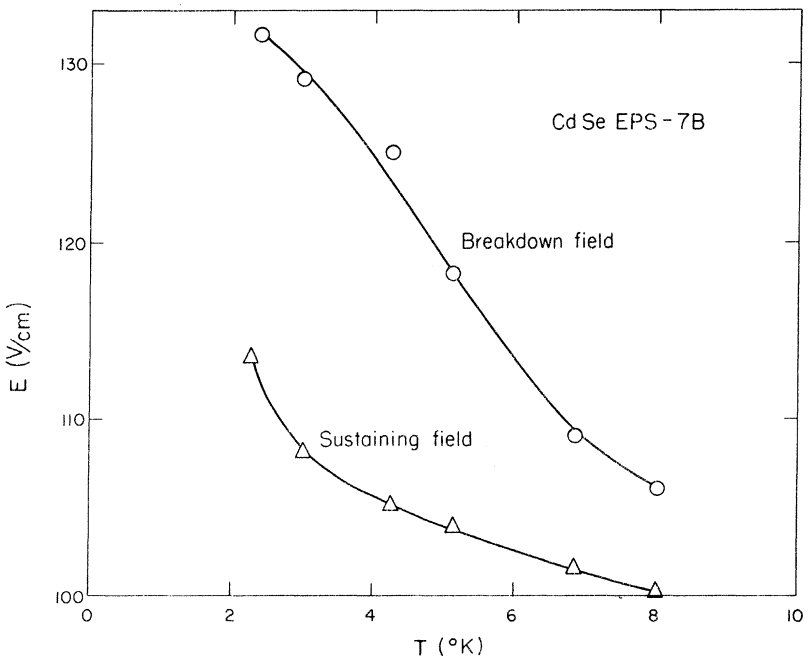

FIG. 7. Values of electric field at the two turning points; the lower the temperature, the larger is the difference between the two points.

continues to increase, and the slope of R_H^{-1} goes to zero, becomes positive, and then rises sharply. This implies that beyond this field, a sufficiently large fraction of the carriers have been transferred from the impurity states to the conduction band so that the Hall coefficient is dominated by the conduction band. At 7.8 °K, similar effects are noticeable, although the decrease in R_H^{-1} is relatively smaller. This decrease in R_H^{-1} completely disappears at 10.4 °K. At this temperature, the conductivity is primarily controlled by the conduction band.

The analysis of the field dependence of the mobility at low temperature is complicated because (i) impurity conduction predominates below breakdown and (ii) current saturation resulting from the acoustoelectric amplification of phonons occurs at or just beyond breakdown. Sample EPS-2, however, had a sufficiently low mobility so that current saturation occurred at about 140 V/cm at about 20 °K; furthermore, at 20 °K, impurity conduction was minimal. The experimental mobilities for 24 and 17.1 °K are compared in Fig. 9 with the theoretical mobility based upon the ETM (see Appendix A). The electron concentration as a function of field needed in the ETM is taken directly from the Hall coefficient, i.e., $n(E) = e^{-1} R_H^{-1}(E)$. At 17.1 °K, current saturation is evident at $E \approx 120$ V/cm. The strong temperature dependence of the mobility at lower electric fields is due to the dominance of ionized-impurity scattering. At higher electron temperatures, ionized-impurity scattering becomes less important, thus reducing the temperature dependence at high fields.

V. PHOTOMULTIPLICATION AND SWITCHING

Under illumination, the threshold field for breakdown decreases and the I-V characteristics are shown in Fig. 10. The data are shown at two temperatures for the sample EPS-3, which has a room-temperature carrier concentration of 3×10^{16} cm^{-3}. At 4.25 °K, the threshold fields under dark and light conditions are 116 and 112 V/cm, respectively. At both temperatures, the photocurrent, which is the difference between the current under illumination and that in the dark, is shown by the dotted line. It is found that at higher fields beyond the CCNR, the value of the photocurrent is that extrapolated from the low-field photocurrent.

In Fig. 11, I-V characteristics of one of the samples are shown under varying intensities of illumination. The intensity of illumination increases progressively, as shown by the curves $L_1 - L_4$. As the intensity of light increases, the threshold field decreases, and at higher intensity the CCNR disappears. Above the second inflection point the curves revert to normal Ohmic behavior.

If the field can be kept constant by using a low-

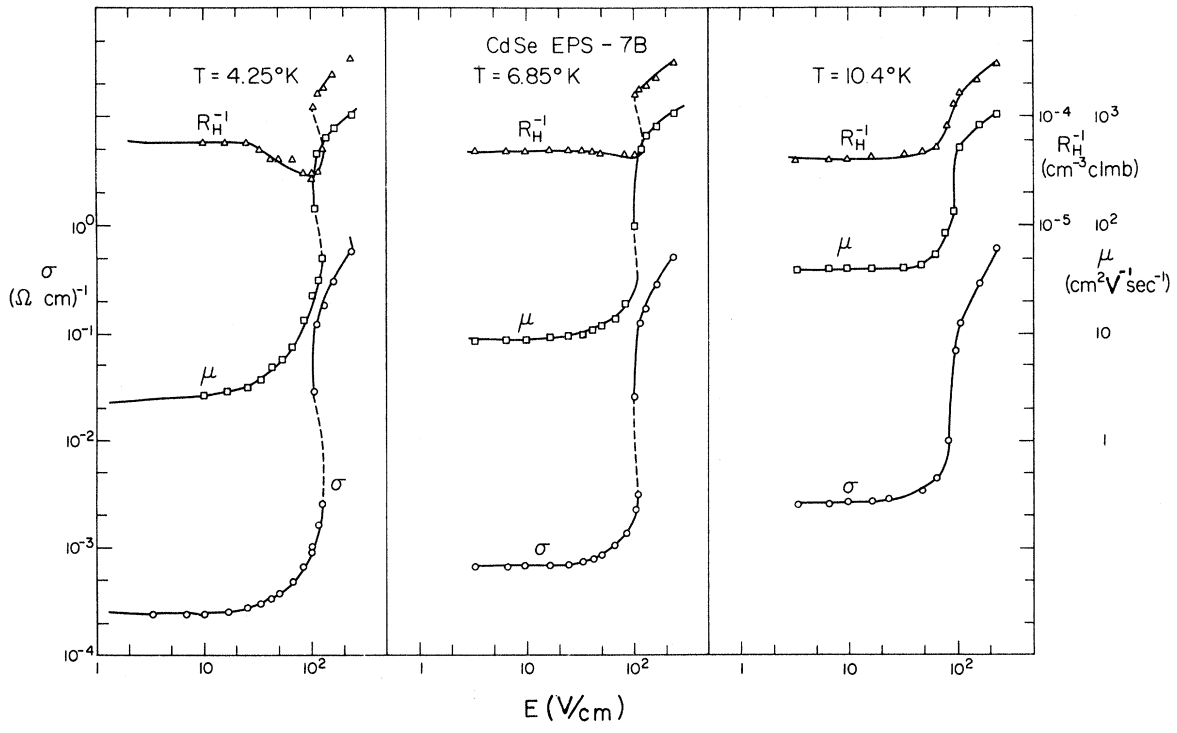

FIG. 8. σ, $(R_H)^{-1}$, and μ vs electric field for the sample EPS-7B at the temperatures indicated.

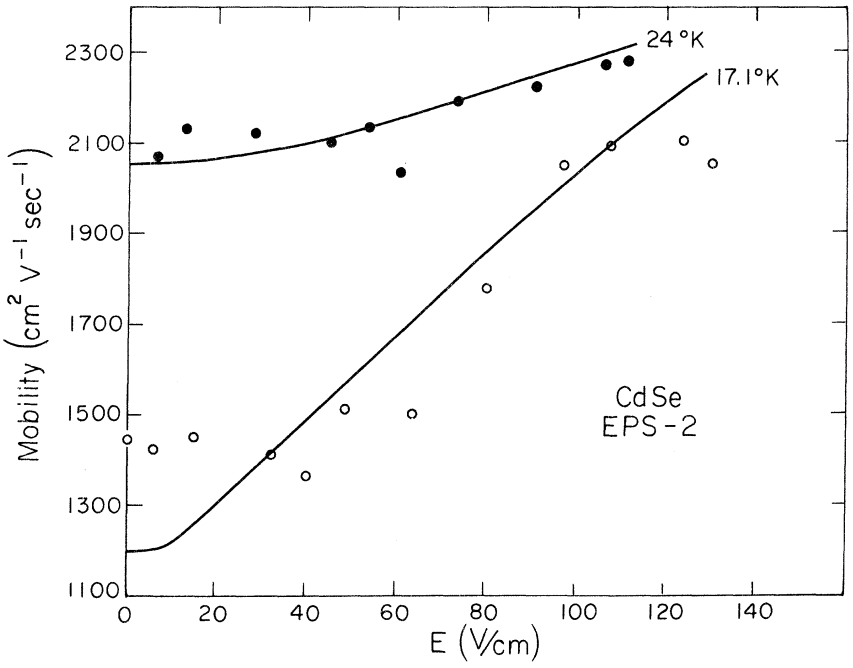

FIG. 9. Mobility vs electric field for EPS-2 at 17.1 and 24°K. Note the drop in mobility beyond 120 V/cm due to current saturation. Solid lines through the data points represent the calculated mobility based upon the electron-temperature model (see text). Although the experimental points are scattered, the quantitative as well as the qualitative agreement is good.

impedance constant-voltage source, then the samples can be switched from a low-current to a high-current state.

The lower trace of Fig. 12 shows the transient photoresponse in the low-field ("Ohmic") region to a short light pulse. The current (upper trace) rises with a response time limited by the light-pulse risetime and decays with two characteristic time constants: One, on the order of 10–20 μsec, is evident here; the other is much longer (10^2–10^4 msec).

The lower curve of Fig. 13, is a plot of photocurrent vs relative intensity in the low-field region. The photocurrent has a linear dependence on light intensity in the Ohmic region. In the high-field region, the decrease in threshold field is intensity dependent and is shown in the upper trace of Fig. 16. The change in threshold field is linear with intensity at low-intensity levels, but at higher intensities ΔE saturates. This situation corresponds to the fact that no CCNR is observable, even though impact ionization is occurring.

The drop in the value of the threshold field under illumination can be utilized to trigger the avalanche and switch the sample from a low- to a high-current state. This is illustrated in Fig. 14. The arrows show the beginning and the end of the 140-μsec pulse. This trace represents the current through the sample. The lower trace shows the delayed light pulse. The sample switches into a high-current state when it is subjected to the light pulse. The high-current state is maintained until the external voltage is turned off. Values of I_{pc}/I_{dark}, where $I_{pc}=I_{light}-I_{dark}$ in the CCNR region can be calculated. These values vary from 8 and 12 at 4.25 and 1.37°K, respectively, for sample EPS-3 in Fig. 13 to ≈ 200 for sample SWC-1 at 4.25 °K in Fig. 11. The value of I_{pc}/I_{dark} of 200 corresponds to $\sim 10^4$ electrons/photon. After the threshold, the photocurrent drops and the value of I_{pc} is negligible.

In Sec. II, we showed that as the temperature increases, the number of carriers in the conduction band increases. This results in a decrease of threshold field for breakdown. Similar arguments apply in the case of carrier concentration under varying intensity of illumination at a fixed temperature. Thus, for a fixed temperature, if the number of carriers is increased with increasing intensity of illumination $L_1 - L_4$, as shown in Fig. 10, the threshold field decreases.

Thus, if a sample is kept at a lower field than the threshold field in the dark, it is possible to cause the breakdown and switch the sample to a high-current state.

VI. DISCUSSION OF IMPACT IONIZATION, BREAKDOWN, AND NEGATIVE RESISTANCE

Various mechanisms for the CCNR have been proposed.[2,3,13–16] An essential feature of these models is the assumption that there exists an energy-loss process which involves scattering of conduction electrons by bound electrons in impurity states. It is suggested that the energy-loss process becomes ineffective once the impact ionization of the shallow donors is initiated.

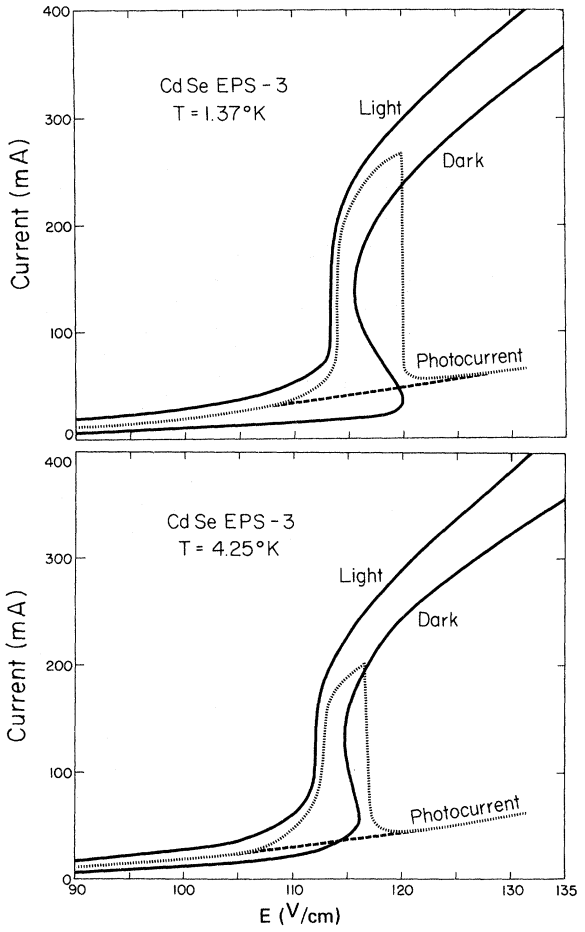

FIG. 10. Effect of illumination in EPS-3 at 4.25 and 1.37 °K. A decrease in the threshold field is evident. The photocurrent peaks at the threshold field in the dark.

McWhorter and Rediker,[2] who observed the negative resistance in Ge, suggested that the source of CCNR is an inelastic scattering of the conduction electrons on a hydrogen-ion molecule. Qualitatively, the scatterer is formed by the sharing of an electron, in n-type material, by two donor atoms, one of which has been previously ionized by a compensating acceptor. Calculations of the rate of energy loss based upon this model have been carried out by Callaway and Cummings.[13] It is expected that as these states are impact ionized, this energy-loss mechanism disappears. An electron bound to a hydrogen-ion molecule may have a different ionization energy (probably larger) than an electron bound to a simple donor. Thus, such a molecule may not be ionized at the same field as the donor.

Zylbersztejn[3] suggested that when the material is strongly compensated, the impurity band is partially empty, even at low temperatures; the charge carriers belonging to it may therefore gain some energy within it. Collisions between the electrons in the conduction band and those in the impurity band may then be efficient enough for the electrons in the conduction band to lose a part of their energy, before they are able to free the impurity-band electrons by means of impact ionization; after the onset of breakdown, the free electrons become much more numerous than the impurity-band electrons, and such collisions are much less probable; the sustaining field becomes lower than the breakdown field.

Yamashita[14] assumed that the mutual interaction between the electrons residing on the donors and the electrons in the conduction band was sufficient-

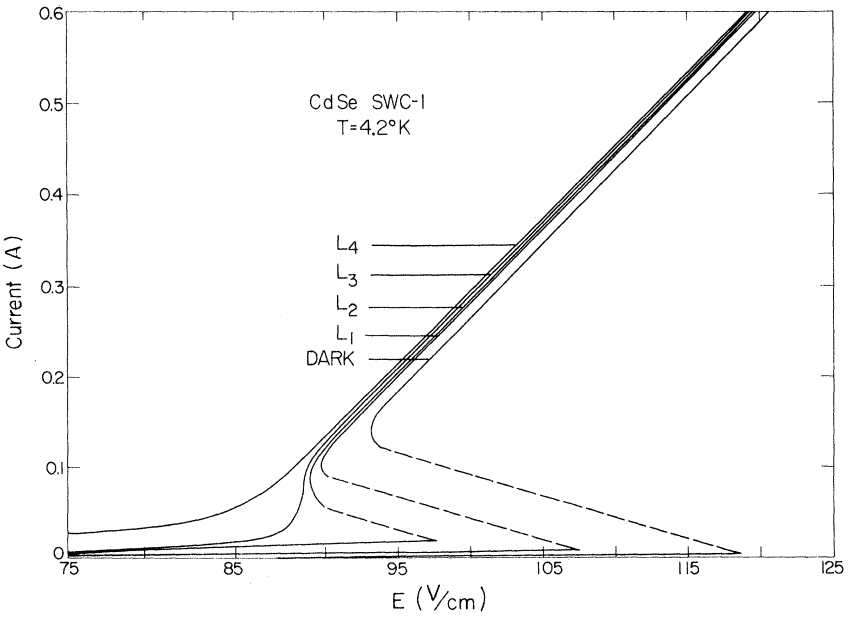

FIG. 11. I-V characteristics of the sample SWC-1 under varying intensity of illumination. The intensity of illumination increases progressively as shown by the curves $L_1 - L_4$.

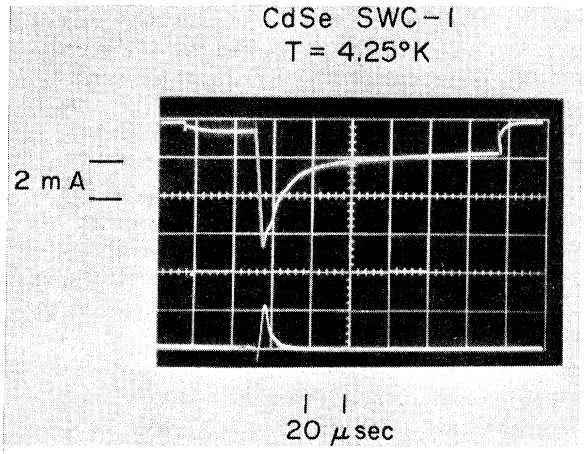

FIG. 12. Transient photoresponse in the low-field (Ohmic) region to a short pulse of light shown in the lower trace. See text for interpretation of rise and decay times.

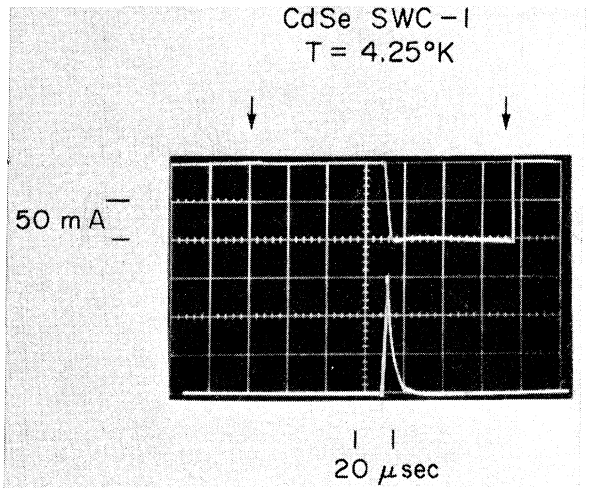

FIG. 14. Photoinduced switching due to decrease in threshold field under illumination. See text for detailed description of the figure.

ly strong to maintain an equilibrium between them. The impurity electrons then dissipate to the lattice the energy supplied to the conduction electrons by the electric field. This energy-loss mechanism becomes less effective as impact ionization proceeds because fewer bound electrons remain to dissipate the energy.

An alternative model is proposed by Kurosawa.[15] He argues that, prior to breakdown, the electron distribution function is determined by the Boltzmann equation (BE), wherein electron-electron scattering is not important, since the conduction-electron density is very small. As the carrier density increases during breakdown, the electron-electron scattering becomes more important, and the electron distribution can be described by the ETM. The BE distribution function is smaller at the impact-ionization threshold energy and is larger at low energy than the ETM distribution function. This implies that with increasing n, the impact-ionization probability increases because the occupation at the threshold energy is greater in the ETM than in the BE distribution function, and the recombination probability decreases because the occupation of low-energy states is smaller in the ETM than BE distribution function. Thus, one expects CCNR to be a consequence of the increasing influence of electron-electron scattering.

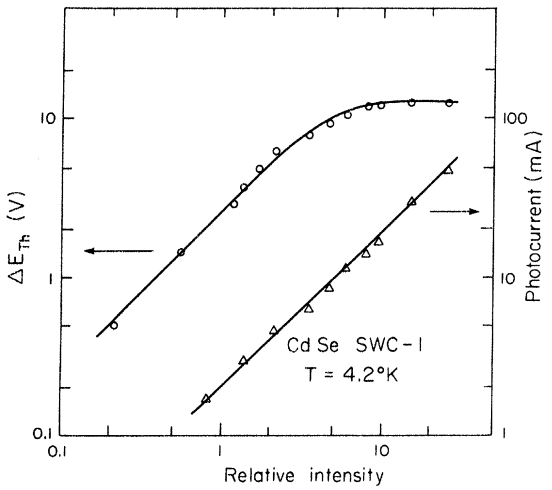

FIG. 13. Photocurrent vs light intensity in the low-field region. $I_{pc} \propto$ light intensity (lower curve). Upper curve represents the change in threshold field vs intensity of illumination.

Crandall[16] developed the screening model in which an increase in carrier concentration in the conduction band due to impact ionization causes a screening of the electron-ionized impurity scattering as well as the electron-phonon interactions. The resulting decrease in electron scattering causes a heating of the electron gas and more impact ionization, which leads to a positive feedback. Therefore, the electric field decreases, while the distribution remains hot, thus maintaining the original state of impact ionization. A quantitative calculation of the breakdown field and the turning points based on screening has not been done, however, because of the difficulties in treating both the recombination process and screening. Crandall considers that the screening affects only the ionized-impurity scattering. The equation for the mobility due to ionized-impurity scattering can be written

$$\mu_{II} = \frac{3\sqrt{2}(k_B T^*)^{3/2}\epsilon_0^2}{4\pi\sqrt{m^*}e^3(n+N_A)} \ln\left(\frac{2m^*\epsilon_0(k_B T^*)^2}{\hbar^2\pi n e^2}\right), \quad (5)$$

if $2m^*\epsilon_0(k_BT^*)^2 \gg \hbar^2\pi me^2$. For small n, i.e., $n < N_A$, the n dependence of the ln term dominates and μ_{II} increases with increasing n. This results in CCNR.

Crandall attributed the second turning point to the fact that, as impact ionization proceeds, n will be reached such that $n \approx N_A$. At this point, the increase in impurity scattering counteracts the screening and terminates the CCNR. Our experimental data show that n and μ continue to increase after the second turning point (see Fig. 8).

Screening of the donor energy levels provides another mechanism for generating CCNR. The increasing conduction-band electron density that occurs during breakdown provides increased screening for the remaining unionized donors. All the donor energy levels are shifted toward the conduction-band edge. The ionization energy is reduced, thus making impact ionization more likely.

The preceding five mechanisms for producing CCNR all involve impact ionization of the donor states. They all have one common aspect, namely, G_I, the impact-ionization probability, is an increasing function of n for constant electric field in the breakdown region. We will show qualitatively how this dependence of G_I on n gives rise to the CCNR. No attempt will be made to calculate $G_I(n, E)$ from a microscopic theory. Each of the five mechanisms discussed above must be treated separately. We will assume only that G_I is an increasing function of n at constant field. Indeed, the low-temperature CCNR may result from a combination of the mechanisms listed above.

Following Koenig,[17] the rate equation for the conduction-band electron density can be written

$$\frac{dn}{dt} = n(N_D - N_A - n)\,G_I + (N_D - N_A - n)\,G_T - n(N_A + n)\,R_T - n^2(N_A + n)\,R_A\,, \quad (6)$$

where G_I and G_T are the impact- and thermal-ionization probabilities, respectively, and R_T and R_A are the thermal- and Auger-recombination probabilities, respectively. All may be n and E dependent; however, we wish to consider only the n dependence of G_I. The steady state n is determined by solving the transcendental equation obtained by setting $dn/dt = 0$ in Eq. (6).

The usual criterion for breakdown without CCNR is obtained from the steady-state condition upon neglect of both the n^2 and n^3 terms in Eq. (6) and the n dependence of G_I. Then,

$$n = \frac{G_T(N_D - N_A)}{R_T N_A - G_I(N_D - N_A)}\,. \quad (7)$$

With increasing electric field, G_I increases until the denominator approaches zero. This implies breakdown without CCNR.[17]

We propose that the CCNR can be viewed as follows. At the breakdown field, the conduction-band electron density increases very rapidly for a small increase in the electric field. The steady state n does not, however, proceed to infinity, but does increase only until the quadratic terms in Eq. (6) become important, thus limiting further increase. Auger recombination is usually not important in low-temperature impact ionization. Then, in the steady state, the solution of Eq. (6) is

$$n = -\frac{G_T + N_A R_T - (N_D - N_A)\,G_I}{2(G_I + R_T)} + \frac{\{[G_T + N_A R_T - (N_D - N_A)\,G_I]^2 + 4(G_I + R_T)(N_D - N_A)\,G_I\}^{1/2}}{2(G_I + R_T)}\,. \quad (8)$$

Figure 15 shows n plotted schematically vs G_I for three different lattice temperatures T_1, T_2, and T_3, where $T_1 < T_2 < T_3$. For very small G_I, thermal equilibrium prevails and $n = (G_T/R_T) \times (K^{-1} - 1)$. For very large G_I, corresponding to a high electric field, n approaches $N_D - N_A$. If G_I is a monotonically increasing function of electric field, and is independent of n, then CCNR will not occur.

If G_I is an increasing function of n, then CCNR may occur. This is shown schematically in Fig. 15 for several values of the electric field E_1, E_1', E_2, E_2', and E_3, where $E_1 > E_1' > E_2 > E_2' > E_3$. At a given temperature T_1 and for a given value of the electric field E_1, the steady-state solutions of the rate equation are given by the intersection of the curves marked T_1 and E_1. For this case, two steady-state solutions exist. More generally, for small values of E, such as E_3, G_I is very small, and only one solution for n exists. For $E_1 \leq E \leq E_2$, either two or three solutions exist, and for $E > E_1$, only one solution exists. Thus, n vs E has the shape depicted in Fig. 16. Since the current is proportional to n, and assuming that the mobility does not contain singularities, the singularities in n become the singularities in current. The fields E_1 and E_2 become the turning points in the S-shape current-vs-field curve. At a higher temperature T_2, the turning points E_1 and E_2 have shifted to lower values E_1' and E_2'. At a still higher temperature T_3, only one steady-state solution exists for all electric fields. In this case, the conduction-band electron density may increase rapidly with electric field, but a region of CCNR will not occur.

The n dependence of G_I for one of the five models, namely, the screening model of Crandall,[16] can be easily ascertained. In Appendix B, the im-

pact-ionization probability for shallow donors G_I is shown to be

$$G_I = \frac{6(2\pi)^{1/2}|F_0|^2 e^4 (k_B T^*)^{1/2}}{\epsilon_0^2 \sqrt{m^*}\, \mathcal{E}_D^2} e^{-\mathcal{E}_D/k_B T^*}, \quad (9)$$

where T^* is a function of both E and n, the n dependence arising from the screening term in μ_{II} [see Eq. (A4)]. For appropriate choices of G_T and R_T, G_I traces out the E curves shown in Fig. 15. Quantitative fits of this model are not possible, however, because the temperature and n dependence of the recombination probability are not known. Further work must be done to be able to distinguish between the various models which give rise to the n dependence of G_I. Only then can the origin of the CCNR be determined for a given material.

VII. SUMMARY AND CONCLUSIONS

Low-electric-field conductivity, Hall-coefficient, and mobility measurements on several CdSe samples yield a systematic decrease in the donor ionization energy from 18 to 10 meV with increasing impurity concentration. The sample with the lowest impurity concentration has the donor ionization energy expected from the effective-mass model. The low-field mobility is determined by both ionized- and neutral-impurity scattering at low temperature and by polar optical-phonon scattering at high temperature. The theoretical mobility based upon the electron-temperature model fits the experimental mobility from 20 to 300 °K.

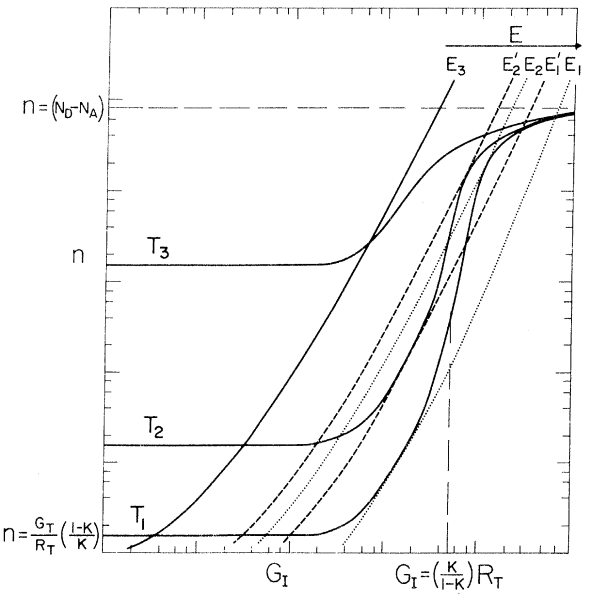

FIG. 15. n vs G_I from Eq. (8) in the text for three temperatures T_1, T_2, and T_3, where $T_1 < T_2 < T_3$. Observance of CCNR depends on the value of the electric field and the temperature (see text for details).

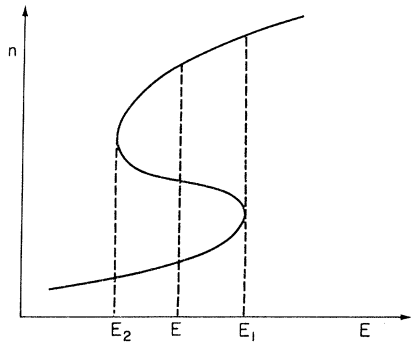

FIG. 16. n vs E from the steady-state solutions of the rate Eq. (6), as described in the text.

For an electric field of about 100 V/cm for $T \lesssim 10$ °K, electrons are transferred from the donor states to the conduction band by impact ionization. A region of CCNR occurs. The high-field mobility calculated within the electron-temperature model agrees reasonably well with the experimental mobility. Several models for the CCNR are discussed, but further work must be done in order to determine the correct model.

Illumination causes the sample to switch to the high-conductivity state if it is biased just below the threshold for the onset of CCNR.

ACKNOWLEDGMENT

We are grateful to Dr. D. L. Losee for various discussions during the course of this work and for useful comments on the manuscript.

APPENDIX A

The conduction-band electron distribution function within the electron-temperature model (ETM) in the diffusion approximation is

$$f(\vec{k}) = \Omega\left(1 + \frac{\hbar^2 \vec{k}\cdot\vec{k}_0}{m^* k_B T^*}\right) e^{-\hbar^2 k^2/2m^* k_B T^*}, \quad (A1)$$

where the electron temperature T^*, and the drift-wave vector $\vec{k}_0$ are determined from the first two moments of the Boltzmann equation. If the electrons scatter from ionized and neutral impurities, polar optical phonons, and acoustic phonons via both the piezoelectric and deformation potentials, then, as is well known, the total mobility μ_T is exactly

$$\mu_T^{-1} = \mu_{PO}^{-1} + \mu_{DP}^{-1} + \mu_{PZ}^{-1} + \mu_{II}^{-1} + \mu_{NI}^{-1}, \quad (A2)$$

where

$$\mu_{PO} = \frac{3(\pi k_B T^*)^{1/2}}{2(2m^*)^{1/2} E_0 N_{PO}} \left[\frac{\gamma}{2}(1 - e^{\gamma_0 - \gamma}) e^{\gamma/2} K_0\left(\frac{\gamma}{2}\right) + (1 + e^{\gamma_0 - \gamma})\frac{\gamma}{2} e^{\gamma/2} K_1\left(\frac{\gamma}{2}\right)\right], \quad (A3)$$

$$\mu_{II}=\frac{3\sqrt{2}(k_BT^*)^{3/2}\epsilon_0^2}{4\sqrt{\pi}\sqrt{m^*}N_I e^3}\left[-1-\left(1+\frac{\hbar^2}{8m^*\lambda^2 k_BT^*}\right)\times e^{\hbar^2/8m^*\lambda^2k_BT^*}\,Ei\left(\frac{\hbar^2}{8m^*\lambda^2k_BT^*}\right)\right]^{-1}, \quad \text{(A4)}$$

$$\mu_{DP}=\frac{3\pi^{3/2}\rho e\, v_l^2\hbar^4}{8\sqrt{2}\,(m^*)^{5/2}E_1^2 k_BT\,(k_BT^*)^{1/2}}, \quad \text{(A5)}$$

$$\mu_{PZ}=\frac{3\hbar^2(k_BT^*)^{1/2}\rho\,\epsilon_0^2}{16(2\pi)^{1/2}(m^*)^{3/2}e\,k_BT}\left\langle\frac{\mu^2}{p^2}\right\rangle, \quad \text{(A6)}$$

$$\mu_{NI}=e^3 m^*/20\hbar^3\epsilon_0 N_{NI}. \quad \text{(A7)}$$

The electron temperature as a function of electric field E is determined by

$$\mu_T E^2=\left.\frac{\delta\mathcal{E}}{\delta t}\right|_{PO}+\left.\frac{\delta\mathcal{E}}{\delta t}\right|_{DP}+\left.\frac{\delta\mathcal{E}}{\delta t}\right|_{PZ}, \quad \text{(A8)}$$

where the terms on the right-hand side of Eq. (A8) represent the net rate at which an electron loses energy to polar-optical phonons and to acoustic phonons via both the deformation potential and the piezoelectric potential, and are

$$\left.\frac{\delta\mathcal{E}}{\delta t}\right|_{PO}=\frac{2E_0N_{PO}\hbar\omega}{(2\pi)^{1/2}\sqrt{m^*}\,(k_BT^*)^{1/2}}\{1-e^{\gamma_0-\gamma}\}\,e^{\gamma/2}K_0\left(\frac{\gamma}{2}\right), \quad \text{(A9)}$$

$$\left.\frac{\delta\mathcal{E}}{\delta t}\right|_{DP}=\frac{8\sqrt{2}\,E_1^2(m^*)^{5/2}(1-T/T^*)(k_BT^*)^{3/2}}{\pi^{3/2}e\rho\hbar^4}, \quad \text{(A10)}$$

and

$$\left.\frac{\delta\mathcal{E}}{\delta t}\right|_{PZ}=\frac{16(2\pi)^{1/2}e(m^*)^{3/2}(1-T/T^*)(k_BT^*)^{1/2}}{\hbar^2\epsilon_0^2\rho}\langle p^2\rangle. \quad \text{(A11)}$$

The mobility μ_T and $\delta\mathcal{E}/\delta t|_{PO}$, $\delta\mathcal{E}/\delta t|_{DP}$, and $\delta\mathcal{E}/\delta t|_{PZ}$ are determined for a given T^*, and the corresponding electric field is then obtained from Eq. (A8). The average piezoelectric constants appearing in $\delta\mathcal{E}/\delta t|_{PZ}$ and μ_{PZ} are determined by a spherical average following Hutson,[18] and the elastic constants are determined by a spherical average following Zook[19]:

$$\langle p^2\rangle=(e^2_{rrr})_{av}+(e^2_{r\theta r})_{av},$$

$$\left\langle\frac{p^2}{\rho\mu^2}\right\rangle=\frac{(e^2_{rrr})_{av}}{\bar{c}_l}+\frac{(e^2_{r\theta r})_{av}}{\bar{c}_t}, \quad \text{(A12)}$$

where

$$(e^2_{rrr})=\tfrac{1}{7}e^2_{33}+\tfrac{4}{35}e_{33}(e_{31}+2e_{15})+\tfrac{8}{105}(e_{31}+2e_{15})^2,$$

$$(e^2_{r\theta r})=\tfrac{2}{35}(e_{33}-e_{31}-e_{15})^2+\tfrac{16}{105}e_{15}(e_{33}-e_{31}-e_{15})+\tfrac{16}{35}e^2_{15},$$

$$\bar{c}_t=c_{44}+\tfrac{2}{15}(c_{11}+c_{33}-2c_{13}-4c_{44}),$$

$$\bar{c}_l=\tfrac{1}{3}(2c_{11}+c_{33})-\tfrac{2}{15}(c_{11}+c_{33}-2c_{13}-4c_{44}).$$

In practice, if the elastic constants are not known, they are approximated by $\bar{c}_l=\rho v_l^2$ and $\bar{c}_t=\rho v_t^2$. The dielectric constants are isotropic and are approximated by[20]

$$\epsilon=\tfrac{1}{3}(\epsilon_{11}+2\epsilon_{\perp}).$$

The screening length λ, which appears in μ_{II}, is

$$\lambda^2=k_B\epsilon T^*/4\pi N_S e^2.$$

We shall assume $N_S=n$ and $N_I=2N_A+n$. In these formulas, $\gamma=\Theta/T^*$ and $\gamma_0=\Theta/T$, where Θ is the temperature equivalent of the polar phonon energy, $N_{PO}=(\exp\Theta/T-1)^{-1}$, K_0 and K_1 are Bessel functions, Ei is the exponential integral, ϵ_0 and ϵ_∞ are the static and high-frequency dielectric constants, ρ is the mass density, v_l and v_t are longitudinal and transverse sound velocities, E_1 is the deformation potential, ω is the polar-optical phonon frequency, m^* is the electron effective mass, and k_B is the Boltzmann constant. The material parameters appropriate to CdSe are listed in Table III. The ETM is discussed by Stratton.[24] Both μ and $\delta\mathcal{E}/\delta t|_{PO}$ can be found in Ref. 24. μ_{NI} is the Erginsoy formula.[25] μ_{II}, μ_{DP}, μ_{PZ}, $\delta\mathcal{E}/\delta t|_{DP}$, and $\delta\mathcal{E}/\delta t|_{PZ}$ are readily determined by using the matrix elements for the appropriate scattering mechanism to calculate the collision integral.[26] Equipartition for the acoustic phonons has been assumed, and all formulas are written in cgs units.

APPENDIX B

The rate of change of n due to impact ionization $n(N_D-N_A-n)G_I$ has been calculated by Cohen and Landsberg.[27] These authors derived the probability

TABLE III. CdSe constants used in calculations.

Symbol	Value	Ref.
m^*	0.21	20
Θ	302 °K	21
$\epsilon_\infty^{\parallel}$	6.3	21
$\epsilon_\infty^{\perp}$	6.2	21
$\epsilon_0^{\parallel}$	10.2	21
$\epsilon_0^{\perp}$	9.33	21
ρ	5.81 g/cm^3	21
v_l	3.8×10^5 cm/sec	21
v_t	1.5×10^5 cm/sec	22
e_{33}	0.347 C/m^2	23
e_{31}	−0.160 C/m^2	23
e_{15}	−0.138 C/m^2	23
$\hbar\omega$	0.026 eV	21
E_1	11.5 eV	20

per unit un-ionized-impurity density per second $P_{\vec{k}}$) that a carrier in state $\vec{k}$ causes the impact ionization of an unionized donor. The total impact-ionization rate is then

$$n(N_D - N_A - n)G_I = n \sum_{\vec{k}} P_{\vec{k}} f(\vec{k}) ,$$

where

$$P_{\vec{k}} = \begin{cases} \dfrac{8\pi m^* e^4 (N_D - N_A - n)|F_0|^2}{\hbar^3 \epsilon_0^2 k_D^3} \dfrac{k^2 - k_D^2}{k_D^2} , & k \geq k_D \\ 0 , & k < k_D \end{cases} \tag{B1}$$

where k_D is such that $\hbar^2 k_D^2/(2m^*) = \mathcal{E}_D$, where $\mathcal{E}_D$ is the ionization energy or donor depth. Within the ETM, $f(\vec{k})$ is a Boltzmann distribution. Then

$$G_I = \frac{16\sqrt{\pi}\, e^4 |F_0|^2 m^*}{\hbar^3 \epsilon_0^2 k_D^3 (k_B T^*)^{3/2}} \int_{\mathcal{E}_D}^{\infty} \sqrt{\mathcal{E}} \left(\frac{\mathcal{E} - \mathcal{E}_D}{\mathcal{E}_D}\right)^2 e^{-\mathcal{E}/k_B T^*} d\mathcal{E} . \tag{B2}$$

The expression for $P_{\vec{k}}$ is the zeroth-order approximation and is very good up to $\mathcal{E}/\mathcal{E}_D = 2$; this range of $\mathcal{E}$ is the most important, since $P_{\vec{k}}$ is integrated over a Maxwellian distribution function. The integral in Eq. (B2) can be done, with the result

$$G_I = \frac{16\sqrt{\pi}\,|F_0|^2 e^4 m^*}{\epsilon_0^2 (2m^* \mathcal{E}_D)^{3/2}} \left[\left(\frac{k_B T^*}{\mathcal{E}_D}\right)^2 \Gamma\left(\frac{7}{2} , \frac{\mathcal{E}_D}{k_B T^*}\right) - 2\left(\frac{k_B T^*}{\mathcal{E}_D}\right) \Gamma\left(\frac{5}{2} , \frac{\mathcal{E}_D}{k_B T^*}\right) + \Gamma\left(\frac{3}{2} , \frac{\mathcal{E}_D}{k_B T^*}\right)\right] , \tag{B3}$$

where $\Gamma(\alpha, X)$ is the incomplete Γ function. These can be expanded for $\mathcal{E}_D/k_B T^* \gg 1$, yielding

$$G_I = \frac{6(2\pi)^{1/2} |F_0|^2 e^4 (k_B T^*)^{1/2}}{\epsilon_0^2 \sqrt{m^*}\, \mathcal{E}_D^2} e^{-\mathcal{E}_D/k_B T^*} . \tag{B4}$$

F_0 is an overlap integral of the lattice periodic part of the Bloch functions for the bound and free electron. Since its value is unknown, it is taken as unity, i.e., $|F_0|^2 = 1$, following Cohen and Landsberg.[27]

[1]S. H. Koenig, Phys. Rev. **110**, 986 (1958).
[2]A. L. McWhorter and R. H. Rediker, Proc. IEEE **47**, 1207 (1959).
[3]A. Zylbersztejn, J. Phys. Chem. Solids **23**, 297 (1962).
[4]P. J. Oliver, Phys. Rev. **127**, 1045 (1962).
[5]R. S. Crandall, Phys. Rev. B **1**, 730 (1970).
[6]R. S. Crandall, Phys. Rev. **169**, 577 (1968).
[7]R. S. Crandall, Phys. Lett. A **32**, 479 (1970).
[8]J. E. Rowe and R. A. Forman, J. Appl. Phys. **38**, 1917 (1968).
[9]H. Fritzsche, J. Phys. Chem. Solids **6**, 69 (1958).
[10]C. H. Henry, K. Nassau, and J. W. Shiever, Phys. Rev. B **5**, 458 (1972).
[11]R. A. Burmeister, Jr. and D. A. Stevenson, Phys. Status Solidi **24**, 683 (1967).
[12]R. A. Reynolds, Solid-State Electron. **11**, 385 (1968).
[13]J. Callaway and F. W. Cummings, Phys. Rev. **126**, 5 (1962).
[14]J. Yamashita, J. Phys. Soc. Jap. **16**, 720 (1961).
[15]T. Kurosawa, J. Phys. Soc. Jap. **20**, 1405 (1965).
[16]R. S. Crandall, J. Phys. Chem. Solids **31**, 269 (1970).
[17]S. H. Koenig, Phys. Rev. **110**, 986 (1958).
[18]A. R. Hutson, J. Appl. Phys. Suppl. **32**, 2287 (1961).
[19]J. D. Zook, Phys. Rev. **136**, A869 (1964).
[20]D. L. Rode, Phys. Rev. B **2**, 4036 (1970).
[21]M. Neuberger, II-VI Semiconducting Compounds Data Tables, Hughes Aircraft Co., 1969 (unpublished).
[22]S. Yee, A. Kawai, and M. L. Neudorfer, Solid-State Electron. **12**, 191 (1969).
[23]D. Berlincourt, H. Jaffe, and L. R. Shiozawa, Phys. Rev. **129**, 1009 (1963).
[24]R. Stratton, Proc. R. Soc. A **246**, 406 (1958).
[25]C. Erginsoy, Phys. Rev. **79**, 1013 (1950).
[26]E. M. Conwell, in *Solid State Physics*, edited by F. Seitz, D. Turnbull, and H. Ehrenreich (Academic, New York, 1967), Suppl. 9.
[27]M. E. Cohen and P. T. Landsberg, Phys. Rev. **154**, 683 (1967).

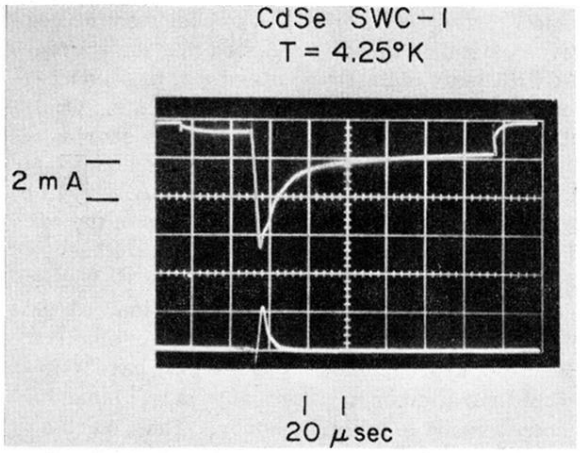

FIG. 12. Transient photoresponse in the low-field (Ohmic) region to a short pulse of light shown in the lower trace. See text for interpretation of rise and decay times.

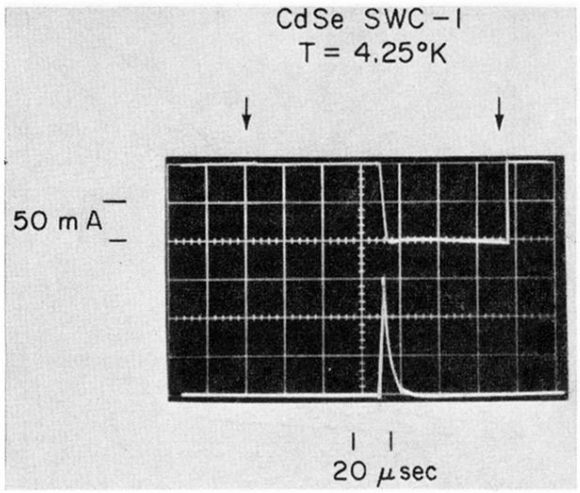

FIG. 14. Photoinduced switching due to decrease in threshold field under illumination. See text for detailed description of the figure.